Experimental report

19/03/2024

Proposal: 1-01-197 **Council:** 10/2022

Title: Synergetic effects of Mn, Ni and Si on RPV embrittlement at high fluences

Research area: Materials

This proposal is a new proposal

Main proposer: Andreas ULBRICHT

Experimental team: Andreas ULBRICHT

Local contacts: Nina-Juliane STEINKE
Sylvain PREVOST

Samples: Steel

Instrument	Requested days	Allocated days	From	To
D33	1	1	13/04/2023	14/04/2023

Abstract:

The proposed SANS experiment is intended to provide macroscopically representative and statistically reliable results of size, volume fraction and number density of irradiation-induced clusters of solute atoms in highly irradiated reactor pressure vessel steels. It serves to clarify possible hardening and embrittlement mechanisms after long term operation.

Synergetic effects of Mn, Ni and Si on RPV embrittlement at high fluences

Introduction / Scientific background

One of the critical issues of long term operation (LTO) of light water reactors, which are the dominant type of the currently operating reactors, is the embrittlement of the reactor pressure vessel (RPV) caused mainly by neutron irradiation. Mn and Ni are alloying elements in RPV steels and they are usually observed in the solute clusters as the origin of irradiation hardening and embrittlement of RPV steels. Many studies indicate that these solute clusters could result from an irradiation-induced mechanism (dragging of solute atoms by point defects). In such a case, a monotonous evolution of the microstructure and hardening with neutron fluence is expected. However, from thermodynamic point of view, Mn, Ni and/or Si can precipitate to form stable phases. In this case, Mn, Ni and Si could result in enhanced hardening and embrittlement at high doses. There is limited understanding on individual as well as synergetic effects of Mn, Ni and Si and associated unfavourable effects on microstructure and mechanical properties in low-Cu RPV steels especially at high fluences. In order to identify a synergetic effect of elements Mn and Ni, low-Mn/low-Ni, high-Mn/low-Ni, low-Mn/high-Ni and high-Mn/high-Ni materials are to be compared and statistically evaluated with respect to mechanical property changes as well as type, composition, volume fraction, number density and size of irradiation-related nano-features.

Experimental

The composition of the investigated materials is summarized in table 1. All the materials were neutron irradiated at an average temperature of 286°C up to an average fluence of $11.1 \times 10^{23} m^{-2}$ under high neutron flux about 2.75×10^{16} $m^{-2}s^{-1}$(E> 1 MeV). The corresponding dose rate and dose are respectively 24.5×10^{-9} dpa s^{-1} and 0.18 dpa (displacements per atom). Plan parallel slices of 1 mm thickness were cut from unirradiated and irradiated condition of tested fracture mechanic specimens of steels A, B, C, F, G and H.

Table 1: Material composition (values in wt%, balance Fe)

Model	C	Si	Mn	Cr	Ni	Mo	V	Cu	S	P
A	0.11	0.28	0.43	2.22	<0.02	0.71	0.10	0.09	0.008	0.010
B	0.11	0.26	0.38	2.19	0.99	0.70	0.10	0.10	0.008	0.010
C	0.12	0.24	0.38	2.13	2.00	0.69	0.10	0.10	0.008	0.010
F	0.12	0.33	1.37	2.15	1.02	0.70	0.10	0.10	0.008	0.010
G	0.11	0.32	1.36	2.06	1.99	0.69	0.10	0.10	0.008	0.009
H	0.12	0.51	1.31	2.07	2.00	0.69	0.10	0.10	0.008	0.010

The SANS experiments were conducted at the instrument D33 using a neutron wavelength of 0.462 nm, a beam diameter of 8 mm and a sample-detector distance of 2 m. During the measurements a saturation magnetic field of 3 Tesla oriented perpendicular to the neutron beam was applied to the samples. Absolute calibration was done using the direct beam method. The ILL software routines (GRASP) were applied to separate magnetic and nuclear scattering cross sections $d\Sigma_{mag}/d\Omega$; $d\Sigma_{nuc}/d\Omega$ from the total cross sections as functions of the momentum transfer vector (also referred to as scattering vector) Q. The size distribution of scatterers was calculated by solving the inverse problem for the measured magnetic difference scattering curves (the scattering curve of the unirradiated condition taken as reference) using the indirect Fourier transform method. Non-magnetic scatterers randomly dispersed in the ferromagnetic matrix were assumed as an

approximation. Mean size, number density and volume fraction of scatterers were estimated supposing spherical shape. Finally, the ratio of magnetic and nuclear scattering was calculated in terms of the so-called A-ratio, A = 1 + *M*/*N*. where *M* and *N* are the measured magnetic and nuclear difference scattering cross sections, respectively, both integrated over the relevant range of *Q*.

Results

The scattering cross sections measured for the unirradiated reference sample and the irradiated sample of steel B and G are shown in Figs 1 and 2, respectively.

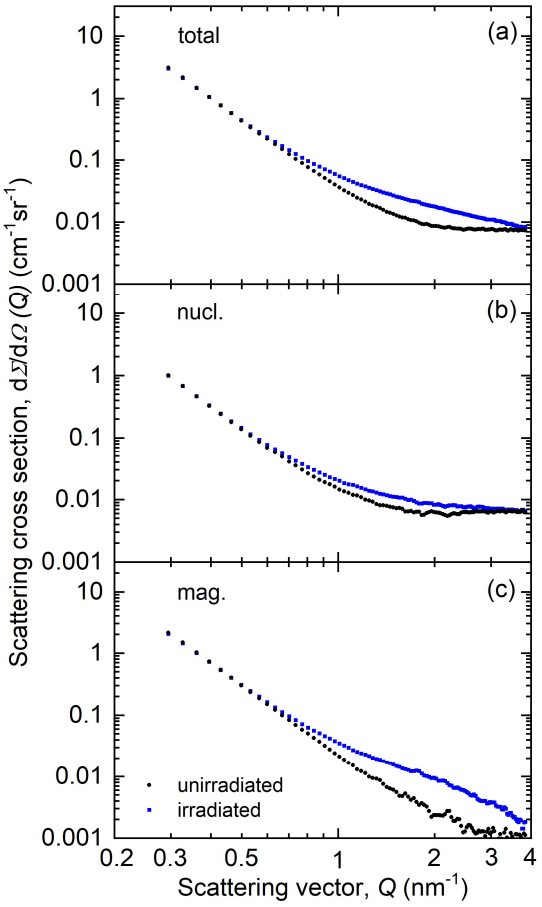

Fig. 1: Measured total (a), nuclear (b) and magnetic (c) scattering cross sections for the unirradiated reference and irradiated conditions of steel B.

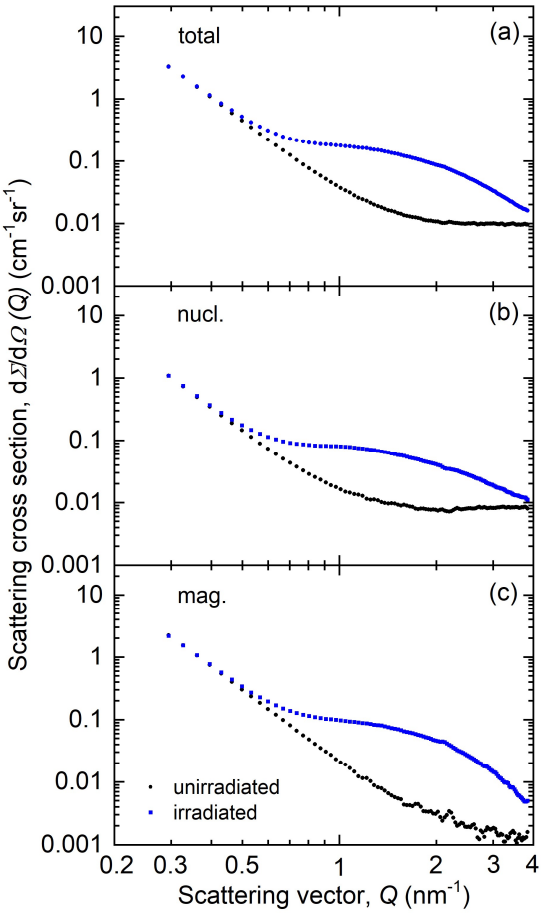

Fig. 2: Measured total (a), nuclear (b) and magnetic (c) scattering cross sections for the unirradiated reference and irradiated conditions of steel G.

An increase in scattering intensity in both the nuclear and magnetic components are observed in the irradiated condition for $Q > 0.5$ nm^{-1} and identical scattering behavior at low *Q*. After deduction of the constant incoherent scattering in the nuclear scattering part (Figs 1(b) and 2(b)), the scattering courses of the magnetic and nuclear scattering are similar. This means the scatterers in the magnetic and nuclear part are the same objects. The scattering intensities caused by the irradiation-induced clusters are clearly represented in Figure 3. The intensities increase with increasing the content of the alloying elements Ni and Mn. The calculated size distributions of these clusters are shown in Figure 4. The characteristics of the irradiation-induced clusters are summarized in Table 2. Increasing of volume fraction of irradiation-induced clusters with an increase of Ni- and Mn-content in the matrix was observed. Increasing the content of just one element (steel C and F) leads to a moderate increase in the cluster fraction. While increasing Ni- and Mn-content causes a doubling of volume

fraction (steel G). This is an indication of a synergetic effect between Ni and Mn. An additional increase in the Si-content in the matrix (steel H) does not cause an additional increase of irradiation-induced clusters, rather a small reduction of cluster volume fraction is observed. There is no obvious dependence of the size of clusters on the Ni, Mn and Si content. Very small cluster radii between 0.55 and 0.72 nm were detected. In comparison, Ni-poor and Cu-containing RPV steels, cluster radii are often in the range of around (1.0 ± 0.2) nm. The A-ratio varies between values of 2 and 4. An increased proportion of Ni in the clusters tends to larger A-ratios and a higher proportion of Mn to lower A-ratios. There is no clear dependence of the A ratio on the material composition and therefore no clear dependence of cluster composition on matrix composition can be seen.

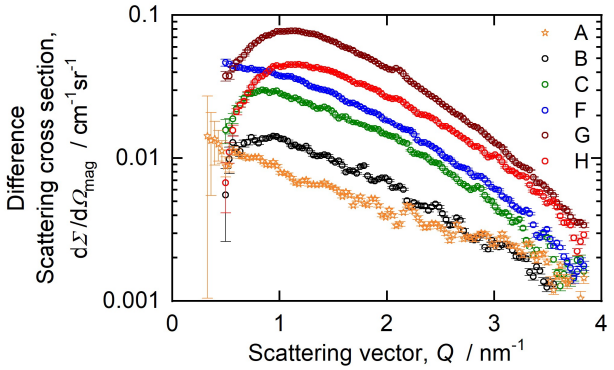

Fig. 3: Measured magnetic difference scattering cross sections of the steels A, B, C, F, G and H with the unirradiated condition subtracted.

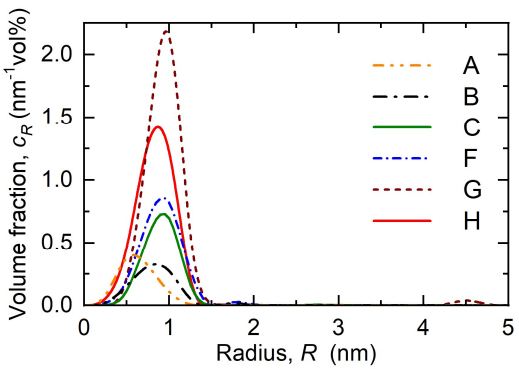

Fig. 4: Size distribution of irradiation-induced scatterers in terms of volume fraction per size increment for the steels, A, B, C, F, G and H.

Table 2: Characteristics of irradiation-induced clusters determined by SANS.

Matrix composition (wt%)				**Parameter of irradiation-induced clusters**			
Steel	**Ni**	**Mn**	**Si**	***c* (vol%)**	***N* (10^{16} cm^{-3})**	***R*$_{mean}$ (nm)**	***A*-ratio**
A	< 0.02	0.4	0.3	0.22 ± 0.06	200 ± 50	0.55 ± 0.03	-
B	1.0	0.4	0.3	0.20 ± 0.01	115 ± 12	0.66 ± 0.04	4.0 ± 0.1
C	2.0	0.4	0.3	0.38 ± 0.01	200 ± 20	0.70 ± 0.04	2.6 ± 0.1
F	1.0	1.3	0.3	0.50 ± 0.02	248 ± 25	0.70 ± 0.04	2.0 ± 0.1
G	2.0	1.3	0.3	1.08 ± 0.02	519 ± 45	0.72 ± 0.04	2.2 ± 0.1
H	2.0	1.3	0.5	0.81 ± 0.02	444 ± 40	0.67 ± 0.04	2.0 ± 0.1

One of the impactful properties of the observed clusters is their capability to act as an obstacle for dislocation slip and, consequently, to efficiently harden the material. The critical shear stress for overcoming the obstacles is proportional to the square root of the volume fraction if the obstacles can be approximated as uniformly sized particles. Fig. 5 illustrates the relationship between the increase in hardness and the volume fraction determined by SANS.

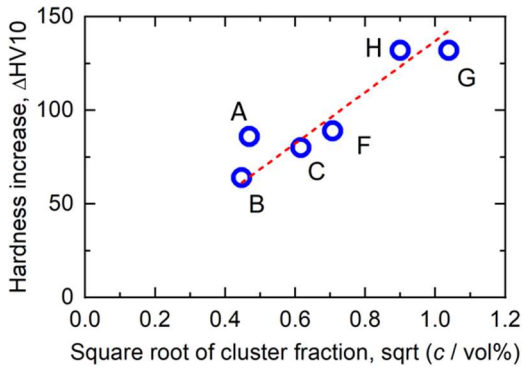

Fig. 5. Correlation between hardness increase and the square root of volume fraction of irradiation-induced clusters.